

A Wide Passband Frequency Selective Surface with Angular Stability



TANG Xingyang¹, SUI Jia¹, FU Jiahui¹, YANG Kaiwen²,
ZHAO Zhipeng²

(1. Harbin Institute of Technology, Harbin 150001, China;
2. ZTE Corporation, Shenzhen 518057, China)

DOI: 10.12142/ZTECOM.202501010

<https://kns.cnki.net/kcms/detail/34.1294.TN.20250225.1143.002.html>,
published online February 26, 2025

Manuscript received: 2023-09-24

Abstract: A wide passband frequency selective surface (FSS) is proposed using a five-layer stacked structure. The proposed structure applies four layers of dielectric plates and five layers of metal patches to provide a passband and exhibits more stable frequency responses and lower insertion loss under wide-angle oblique incidence compared with the typical three-layer metal-dielectric structure. According to the simulation results, the proposed FSS can achieve a passband range of 1.7–2.7 GHz with an insertion loss of less than 0.5 dB and a relative bandwidth of 44.1%, and it can preserve stable transmission characteristics with the incident angle ranging from 0° to 45°.

Keywords: frequency selective surface (FSS); wide bandwidth; low insertion loss

Citation (Format 1): TANG X Y, SUI J, FU J H, et al. A wide passband frequency selective surface with angular stability [J]. *ZTE Communications*, 2025, 23(1): 78 – 84. DOI: 10.12142/ZTECOM.202501010

Citation (Format 2): X. Y. Tang, J. Sui, J. H. Fu, et al., “A wide passband frequency selective surface with angular stability,” *ZTE Communications*, vol. 23, no. 1, pp. 78 – 84, Mar. 2025. doi: 10.12142/ZTECOM.202501010.

1 Introduction

Frequency selective surfaces (FSS) are a periodic array structure composed of metal patch units on the dielectric substrate or aperture elements on the metal screen. FSS arrays are essentially spatial filters that can select the working frequency and polarization mode of electromagnetic waves, such as transverse electric (TE) and transverse magnetic (TM), according to the relationship between electric and magnetic fields and the incident plane^[1–3]. The patch type FSS shows the band-stop characteristic and the aperture type FSS shows the band-pass characteristic. FSS is frequently employed in radomes, antenna reflectors, electromagnetic shielding, etc^[4]. For the radome loaded on the filter antenna, the wave transmission characteristic is mainly determined by the loaded FSS array. FSS is a versatile structure that plays a crucial role in controlling and manipulating electromagnetic waves for various applications, with their characteristics determined by the design of the FSS unit, arrangement period, and dielectric properties of the substrate.

Broadband communication systems have proposed stricter bandwidth requirements in recent years^[5]. The wide passband FSS can achieve low insertion loss electromagnetic wave transmission under a broad band and large angle incidence. Mul-

iple works have studied the design of wide passband FSS. In Refs. [6] and [7], a planar broadband FSS composed of three layers of patches is introduced. It exhibits a relative bandwidth of 42% under vertical incidence, although its insertion loss deteriorates significantly at large angles of incidence. A capped dielectric inserted perforated metallic plate bandpass frequency selective surface is reported in Ref. [8]. It can achieve 40° oblique incident stability with a low profile, but its performance is susceptible to fabrication tolerances. In Ref. [9], a three-dimensional FSS with sharp roll-off sidebands is proposed, which has 62% relative bandwidth and sharp roll-off sidebands under the incident wave of TE polarization modes. The demands of dual polarization applications cannot be met by this 3D FSS since it only supports a single polarization wave. A dual-band FSS alternative solution with a complex manufacturing process and a high-dimensional structure is provided in Ref. [10] and can satisfy the demands of applications involving curved surfaces^[11]. Ref. [12] proposes a broadband FSS load with charged inductance. Based on multi-layer cascaded FSS, the characteristics of broadband, low profile, and miniaturization are achieved by increasing the lumped inductance. A passband with a reflection coefficient below –10 dB was obtained at 0.1 – 1.2 GHz, and a stopband with a transmission coefficient below –10 dB was obtained at 5.8 – 12 GHz. Ref. [13] proposes a relatively simple FSS structure for antenna beam control applications, where the FSS

This work was supported by ZTE Industry-University-Institute Cooperation Funds under Grant No. IA20220800001.

structure utilizes a small number of active components to achieve reconfigurability, good transmission and reflection characteristics required for wireless communication applications. In Ref. [14], the FSS bending effect is considered and the performance of FSS deteriorates with increasing curvature. Few studies have been conducted on broadband oblique-incidence stable FSS, which cannot satisfy communication systems' demands for broadband stable FSS. The goal of this paper is to investigate this issue and propose a better framework.

In this paper, a bandpass FSS with a patch-dielectric cascading structure is proposed. It uses two kinds of circular patches with different radii and cross-slotted patches to achieve three transmission poles in the passband. Simulation results indicate a satisfactory -0.5 dB bandwidth spanning from 1.7 GHz to 2.72 GHz, maintaining angular stability from 0° to 45° . Compared with the three-layer FSS, the designed FSS has a wider passband and better oblique incidence frequency response. The relative bandwidth of this FSS is 45.2%, which has low insertion loss and oblique incident stability under both TE and TM polarization. In the meantime, equivalent circuits are provided to check the accuracy of electromagnetic simulations.

2 Design Principle

The design principle of the angular stability FSS is essentially electromagnetic wave impedance matching under oblique incidences. An electromagnetic wave vector is only along its propagation direction. Assume that the vectors of incident, reflected and transmitted waves are \mathbf{k}_i , \mathbf{k}_r and \mathbf{k}_t , respectively. The incident, reflection and refraction angles are θ_i , θ_r and θ_t .

The phase matching condition on the interface is $\mathbf{k}_i \sin \theta_i = \mathbf{k}_r \sin \theta_r = \mathbf{k}_t \sin \theta_t$, where $\mathbf{k}_i = \mathbf{k}_r = \mathbf{k}_1$, and $\mathbf{k}_t = \mathbf{k}_2$. From the above formula, the Snell's law can be obtained. There are two laws in total, namely, the Snell reflection law and the Snell refraction law. The reflection law states that the reflection angle is equal to the incident angle, that is, $\theta_i = \theta_r$. The law of refraction is expressed as the relationship between the refractive angle and the incident angle, that is, $\sin \theta_t / \sin \theta_i = \mathbf{k}_2 / \mathbf{k}_1$, where $\mathbf{k}_1 = \omega \sqrt{\epsilon_1 \mu_1}$ and $\mathbf{k}_2 = \omega \sqrt{\epsilon_2 \mu_2}$. The Snell's laws reflect the laws of reflection and refraction of electromagnetic waves and have a wide range of applications.

According to the boundary conditions, the polarization characteristics will not change when waves are reflected and refracted on the plane boundary, regardless of whether it is a vertically polarized plane wave or a parallel polarized plane wave. When the electromagnetic wave is oblique incidence, the reflection and transmission coefficients are related to the polarization characteristics of the wave. It is viable to derive the formula for the plane wave's reflection and transmission coefficients with two different polarization characteristics.

$$\Gamma_{\perp} = \frac{\eta_2 \cos \theta_i - \eta_1 \cos \theta_t}{\eta_2 \cos \theta_i + \eta_1 \cos \theta_t} \quad (1),$$

$$\tau_{\perp} = \frac{2\eta_2 \cos \theta_i}{\eta_2 \cos \theta_i + \eta_1 \cos \theta_t} \quad (2),$$

where η_1 and η_2 are the characteristic impedance of medium 1 and medium 2, respectively. Similarly, for parallel polarized plane waves, we obtain that

$$\Gamma_{\parallel} = \frac{\eta_1 \cos \theta_i - \eta_2 \cos \theta_t}{\eta_1 \cos \theta_i + \eta_2 \cos \theta_t} \quad (3),$$

$$\tau_{\parallel} = \frac{2\eta_2 \cos \theta_i}{\eta_1 \cos \theta_i + \eta_2 \cos \theta_t} \quad (4).$$

It is well known that when the electromagnetic wave is oblique incidence on the surface of the medium, partial reflection and partial transmission occur. In particular, Eqs. (1) and (3) demonstrate that, in the case of vertical polarization, when the characteristic impedance of the two media is $\eta_1 / \eta_2 = \cos \theta_i / \cos \theta_t$, the reflection coefficient is equal to 0; in the case of horizontal polarization, when the characteristic impedance of the two media satisfies $\eta_1 / \eta_2 = \cos \theta_i / \cos \theta_t$, the reflection coefficient is equal to 0, and there is no reflected wave. The key to improving the stability of oblique incidence is the matching of wave impedance under oblique incidence.

The wave vector of an electromagnetic wave and the normal vector at the interface of the incident medium form the incident plane. There are two different types of polarized waves in the case of oblique incidence: TE polarization (where the electric field is parallel to the incident plane) and TM polarization (where the magnetic field is parallel to the incident plane). The vector transmission line equation can be used to determine the characteristic impedance of the transmission line for the two polarization modes or the impedance of free space waves for the two polarization modes with oblique incidence.

$$Z^{\text{TE}} = \sqrt{\frac{\mu}{\epsilon}} \frac{1}{\sqrt{1 - \frac{1}{\omega^2 \epsilon_i \mu_n}}} \quad (5),$$

$$Z^{\text{TM}} = \sqrt{\frac{\mu}{\epsilon}} \sqrt{1 - \frac{k_i^2}{\omega^2 \epsilon_n \mu_i}} \quad (6).$$

By substituting the relevant formula and the permeability and permittivity of free space, the characteristic impedance of free space under vertical incidence is 377Ω , and the above formula is simplified to $Z_0^{\text{TM}} = 377 \cos \theta$, $Z_0^{\text{TE}} = 377 / \cos \theta$. The wave vector of electromagnetic waves and the normal vector at

the interface of the incident medium form the incident plane. When the electric field is perpendicular to the incident plane, it is a TE wave; when the magnetic field is perpendicular to the incident plane, it is a TM wave. Fig. 1 shows that the wave impedance of free space under oblique incidence is related to the polarization mode of electromagnetic waves, and the wave impedance of free space under TE and TM modes has the opposite trend with the incident angle.

3 Configuration and Discussion

3.1 FSS Configuration

The multi-layer FSS performs better than the single-layer FSS in terms of bandwidth, oblique incidence transmission coefficients, passband flatness and other factors. In this paper, a multi-layer metal-dielectric stack structure is used to design a broadband oblique-incidence stable FSS. The top and bottom layers feature circular patches, while the middle layer employs cross-shaped slots to provide the first resonance point and control the coupling between the upper and lower layers to generate a second resonance point. The circular patches reduce the effective size variations for oblique incidence. The

cross-shaped slots can minimize changes in the electric field direction. To further increase the number of resonance points, an additional layer of dielectric and patch structures is introduced, resulting in a four-layer dielectric and five-layer patch FSS unit.

As shown in Fig. 2, based on the three-layer patch FSS, a five-layer metal patch structure is proposed to expand the bandwidth and reduce the insertion loss deterioration under oblique incidence. The relative permittivity of each dielectric substrate in designed FSS is 3, and the loss tangent is 0.001 3 @ 10 GHz. This five-layer design has been determined to be a simple and efficient FSS structure through contrasting various patch and analysis structures.

Fig. 2a shows the three-layer FSS, which consists of two layers of circular patches with the same radius and a cross slot in the middle layer to form a resonant structure. This structure typically has two transmission poles available. When the upper patch completely covers the cross slot, the cross slot determines the position of the low-frequency transmission pole, the thickness of the medium controls the distance between the two poles, and the radius of the patch controls the passband frequency. Fig. 2b shows the proposed FSS structure, adding two layers of circular patches with a larger radius to the traditional two-layer circular patch structure to increase the transmission poles and improve the oblique incidence stability. Fig. 2c shows the dimensions of the cross slot in the middle layer.

To achieve better results, we discuss and optimize the main parameters of the structure. Fig. 3a shows the simulation results of the frequency responses with changing length l of the cross slot. It is shown that the length of the cross slot has more effect on the first and second resonant frequencies, and less effect on the third resonant frequency. As l increases from 23.14 mm to 25.14 mm, the first and second transmission poles gradually move away from each other, and the relative bandwidth increases from 42.4% to 47.8%. Similarly, Fig. 3b shows the simulation results of the frequency responses for changing the top patch radius R_1 . Changing R_1 has little effect on the first transmission pole, but significantly affects the second and third poles. When R_1 increases to 15.7 mm, FSS can no longer support a passband.

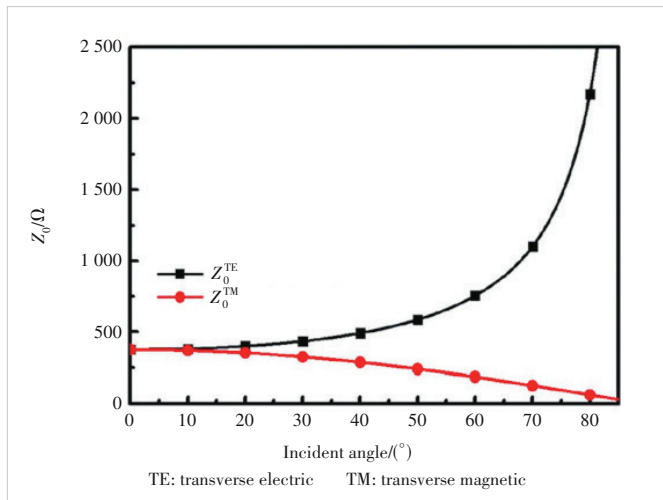


Figure 1. Wave impedance of free space under oblique incidence

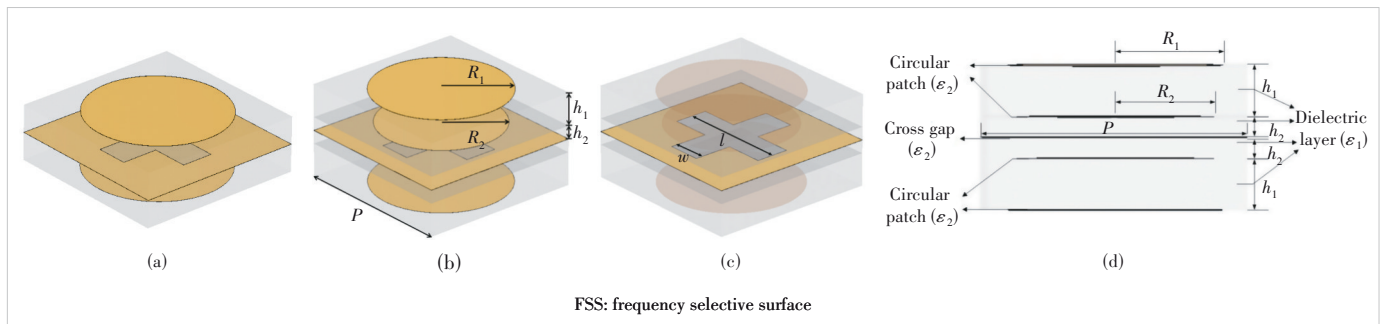


Figure 2. Geometry of the proposed wideband FSS: (a) 3D view of three-layer FSS; (b) 3D view of the proposed FSS (unit: mm; $P = 36$, $R_1 = 14.7$, $R_2 = 13.5$, $h_1 = 7$, and $h_2 = 2.81$); (c) 3D view of the interlayer cross slot of the proposed FSS (unit: mm; $l = 24.14$ and $w = 7.29$); (d) side view

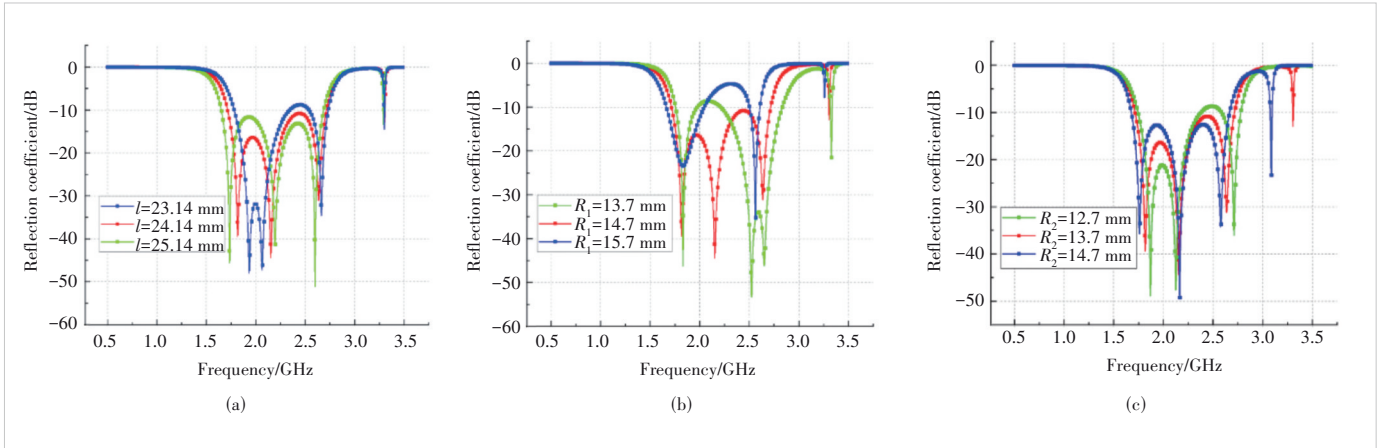


Figure 3. Simulation scattering parameter results of FSS unit cell: (a) results with different cross slot lengths l ; (b) results with different top patch radii R_1 ; (c) results with different middle patch radii R_2

Fig. 3c shows the simulation results of the frequency responses with different middle patch radii R_2 . The value of radius R_2 has less effect on the second transmission pole but more effect on the first and third transmission poles. As R_2 increases, the first and third transmission poles move to lower frequencies, and the relative bandwidth gradually narrows. In addition, the frequency response of FSS is very sensitive to the thickness of the dielectric substrate. Different thicknesses will affect the position of the resonance frequency, bandwidth, oblique incidence performance, etc., so it needs to be considered comprehensively in the design.

3.2 Simulation Results and Discussion

Fig. 4 compares the simulation results of the three-layer FSS and the proposed five-layer FSS. As previously mentioned, the three-layer FSS has a passband from 1.944 GHz to 2.562 GHz, and there are two transmission poles in the passband located at 2.064 GHz and 2.418 GHz, respectively. The relative bandwidth of the conventional FSS is 27.4%. It makes sense that the generated broadband is formed by splicing multiple passbands. The vertical incidence simulation results of the proposed five-layer FSS are also shown in Fig. 4b. The passband is from 1.716 GHz to 2.716 GHz. There are three transmission poles in the band located at 1.816 GHz, 2.152 GHz and 2.64 GHz, respectively, and the relative bandwidth is 45.1%. The designed FSS achieves broadband oblique incidence stable transmission of 1.71 – 2.69 GHz with a thickness as small as possible relative to the center frequency wavelength, a relative bandwidth of 44.5%, and a stable angle of 45° , and supports TE and TM dual polarization. The simulation results for the polarization conversion and insertion loss characteristics of the FSS are displayed in Fig. 5. The FSS demonstrates good performance with minimal polarization conversion and insertion loss. The average insertion loss in the band is less than 0.5 dB, which is at a relatively advanced level in similar works.

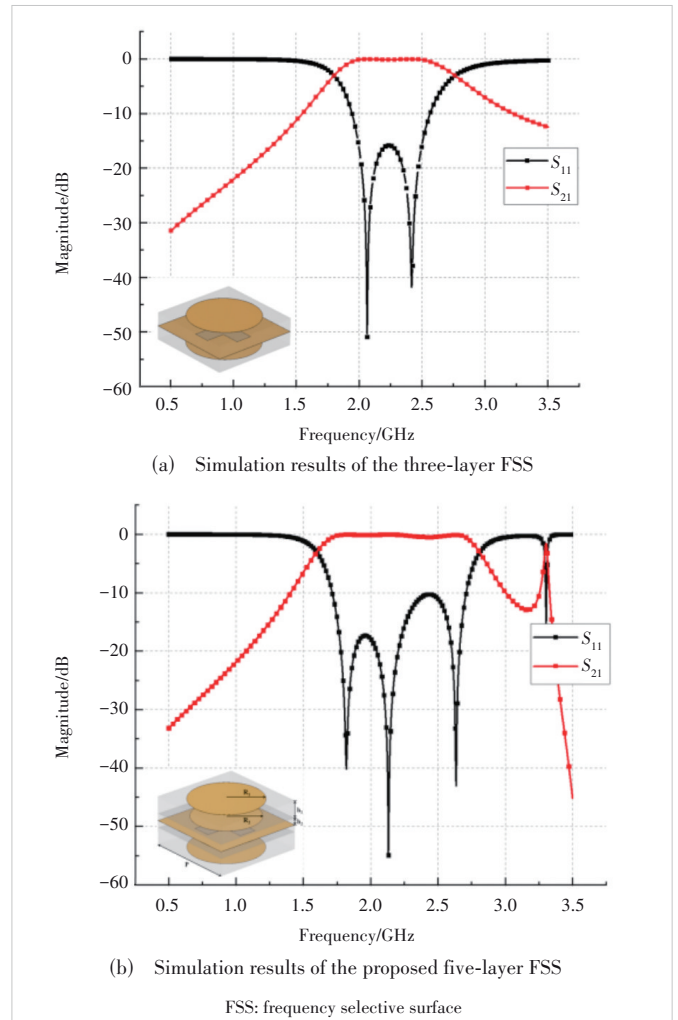


Figure 4. Simulation results of the TE model

To validate the correctness of the designed structure, we extract the equivalent circuit models of the FSS for both the three-layer and five-layer configurations. The results of the

electromagnetic simulations of the equivalent circuits are then compared with those of the circuit simulation. Our proposed structure is reliable and valid, and the results indicate a high level of consistency.

In Fig. 6a, h_1 and h_2 represent two dielectric layers, while Z_{FSS} represents the equivalent circuit of each layer, and they are connected through cascades. In Fig. 6b, L_{m1} represents the equivalent circuit of a circular patch, which is equivalent to an inductance. Considering the coupling relationship with other FSS units, a series capacitor C_{c2} is added; C_{p2} represents the cross gap, equivalent to capacitance; L_{p1} and C_{p1} consist of a series inductor and a parallel capacitor. In addition, it is also necessary to consider the coupling relationship between each layer and add parallel capacitors C_{c1} . The model of the equivalent circuit has been added to Fig. 6.

Different from the three-layer structure, the interlayer coupling effect of the five-layer structure is stronger, so the position of the transmission pole is affected by multiple structural parameters. A more complex model of the five-layer FSS is shown in Fig. 6c.

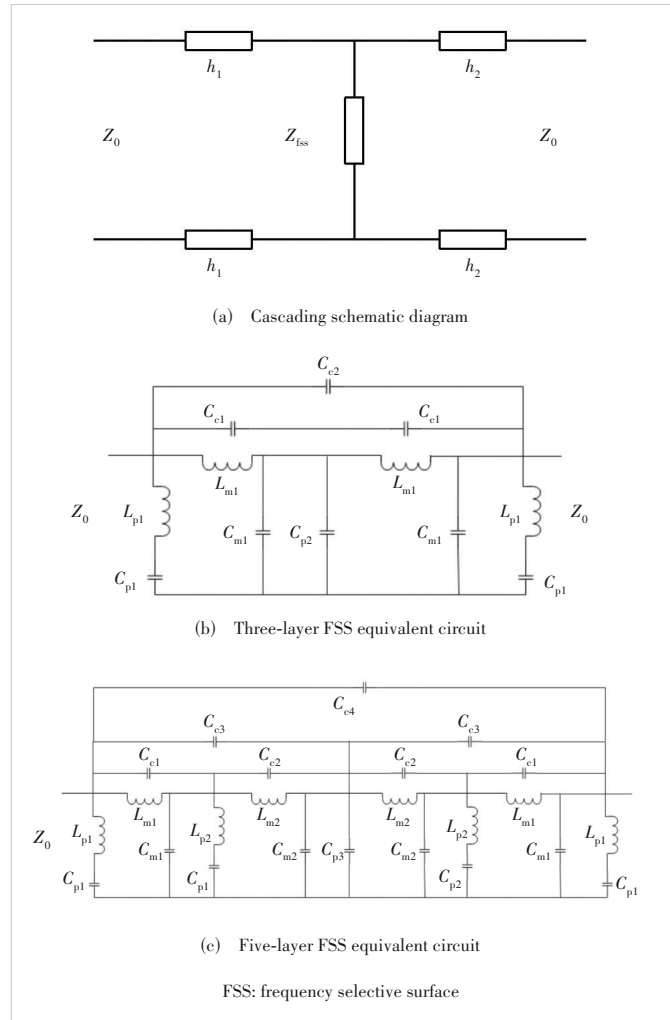


Figure 6. Equivalent-circuit model of FSS

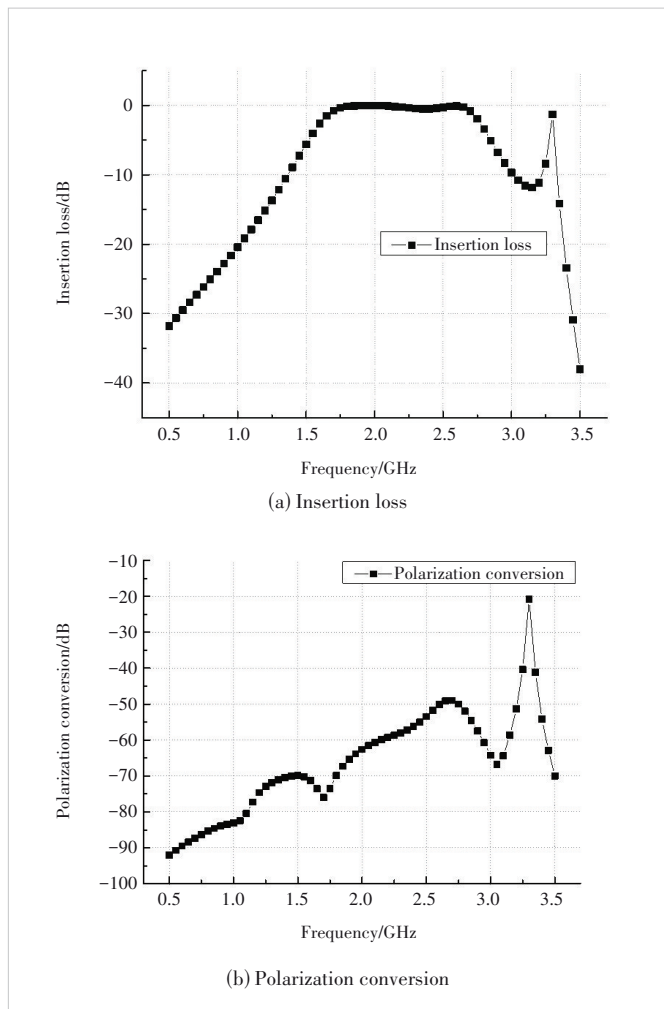


Figure 5. Insertion loss and polarization conversion

Comparing electromagnetic simulation with equivalent circuits in Fig. 7, we find that equivalent circuits can effectively match the FSS model. Comparing the transmission coefficients of the three-layer FSS and the five-layer FSS, we can see that the five-layer FSS has a wider passband.

The frequency response of the FSS unit cell under oblique incidence is shown in Fig. 8. In Fig. 1, as the incident angle changes, the incident impedance also changes in the opposite direction in TE and TM modes. In the TE mode, as the incident angle increases, the first resonant frequency moves to a lower frequency, and the second and third resonant frequencies move to higher frequency. It can be seen that under the 45° oblique incidence, both modes can provide -10 dB bandwidth from 1.71 GHz to 2.7 GHz. The -0.5 dB transmission coefficient bandwidth of FSS is from 1.71 GHz to 2.68 GHz, and the highest insertion loss in the band is 0.48 dB. Under the $0 - 45^\circ$ oblique incidence, FSS can support a relative bandwidth of 44.1% and the trans-

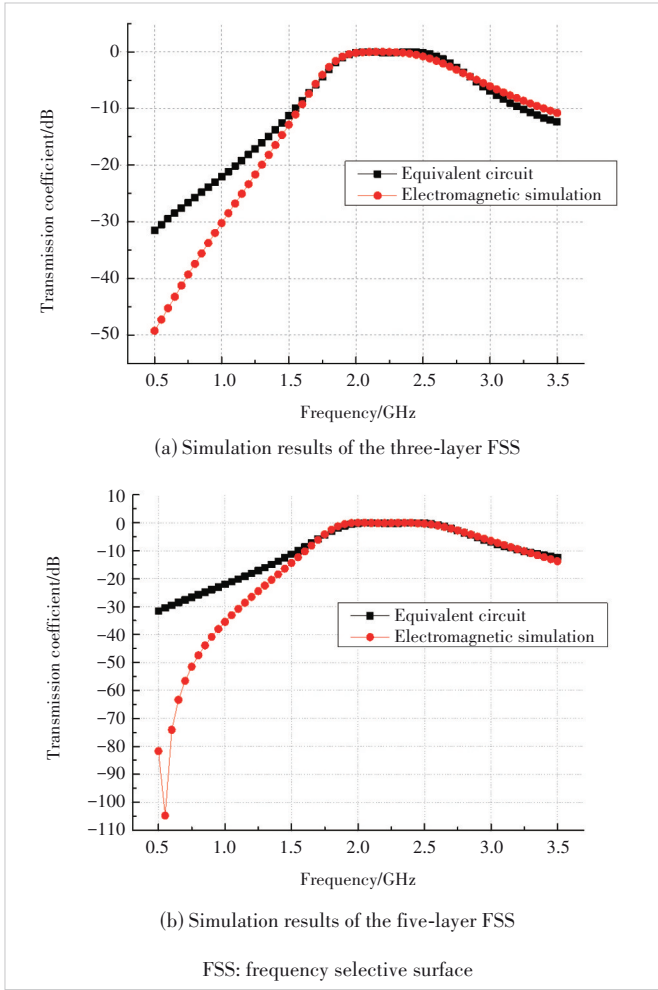


Figure 7. Comparison results of equivalent circuit simulation with electromagnetic simulation

mission coefficient is slightly deteriorated around 1.95 GHz, but still greater than -1 dB. The resonance existing at 3 GHz can be avoided by changing the size of the structure, but doing so will lead to a decrease in performance within the passband. Therefore, we choose to retain the presence of the resonance point at this location.

4 Conclusions

In this paper, a wide passband FSS with angular stability and low insertion loss is proposed. The FSS is designed by a five-layer metal patch stack structure. The upper and lower layers of patches are circular to improve the oblique incidence stability, and the middle layer uses cross slots to control the passband frequency. Simulation results show a wide bandwidth from 1.71 GHz to 2.71 GHz while the insertion loss is less than 0.5 dB. Compared with the three-layer FSS, the designed FSS has a wider passband and better oblique incidence frequency response, which has broad application prospects.

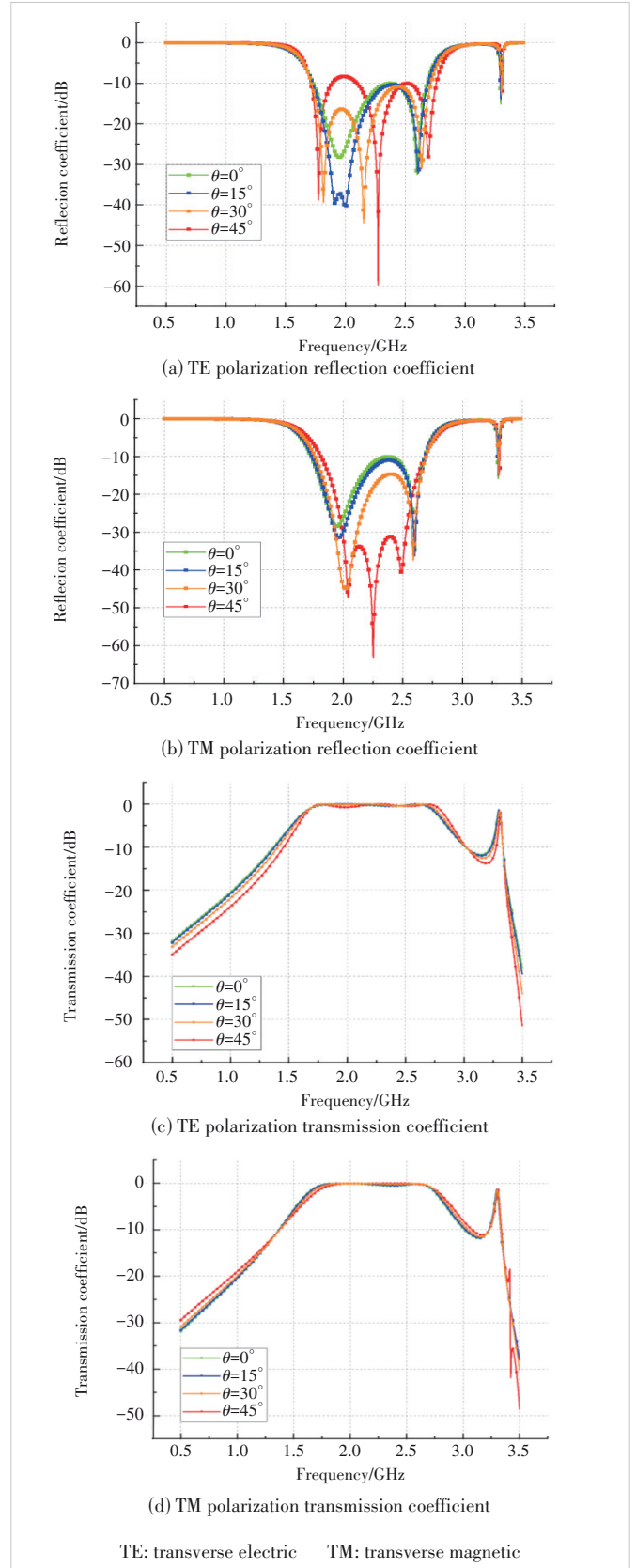


Figure 8. Simulated scattering parameter results of the FSS unit cell under oblique incident angles

References

- [1] MITTRA R, CHAN C H, CWIK T. Techniques for analyzing frequency selective surfaces: a review [J]. *Proceedings of the IEEE*, 1988, 76(12): 1593 – 1615. DOI: 10.1109/5.16352
- [2] MUNK B A. *Frequency selective surfaces: theory and design* [M]. New York, USA: Wiley, 2000. DOI: 10.1002/0471723770
- [3] MUNK B A. *Finite antenna arrays and FSS* [M]. New York, USA: Wiley, 2003. DOI: 10.1002/0471457531
- [4] KURRA L, ABEGAONKAR M P, BASU A, et al. FSS properties of a uniplanar EBG and its application in directivity enhancement of a microstrip antenna [J]. *IEEE antennas and wireless propagation letters*, 2016, 15: 1606 – 1609. DOI: 10.1109/LAWP.2016.2518299
- [5] XU R, LI J Y, WEI K, et al. A broadband slot antenna with unidirectional circularly polarized radiation patterns [J]. *IEEE antennas and wireless propagation letters*, 2016, 16: 317 – 320. DOI: 10.1109/LAWP.2016.2574808
- [6] WANG L L, LIU S B, KONG X K, et al. Frequency-selective rasorber with a wide high-transmission passband based on multiple coplanar parallel resonances [J]. *IEEE antennas and wireless propagation letters*, 2020, 19(2): 337 – 340. DOI: 10.1109/LAWP.2019.2962223
- [7] YANG Z Q, JIANG W, HUANG Q L, et al. A 2.5-D miniaturized frequency-selective rasorber with a wide high-transmission passband [J]. *IEEE antennas and wireless propagation letters*, 2021, 20(7): 1140 – 1144. DOI: 10.1109/LAWP.2021.3073777
- [8] JIN C, LV Q H, WANG J L, et al. Capped dielectric inserted perforated metallic plate bandpass frequency selective surface [J]. *IEEE transactions on antennas and propagation*, 2017, 65(12): 7129 – 7136. DOI: 10.1109/TAP.2017.2764524
- [9] WANG P, JIANG W, HONG T, et al. A 3D wide passband frequency selective surface with sharp roll-off sidebands and angular stability [J]. *IEEE antennas and wireless propagation letters*, 2022, 21(2): 252 – 256. DOI: 10.1109/LAWP.2021.3126890
- [10] WEI P S, CHIU C N, CHOU C C, et al. Miniaturized dual-band FSS suitable for curved surface application [J]. *IEEE antennas and wireless propagation letters*, 2020, 19(12): 2265 – 2269. DOI: 10.1109/LAWP.2020.3029820
- [11] LI T W, FAN Y D, GU Y J, et al. A novel miniaturized multiband strong coupled-FSS structure insensitive to almost all angles and all polarizations [J]. *IEEE transactions on antennas and propagation*, 2021, 69(12): 8470 – 8478. DOI: 10.1109/TAP.2021.3063351
- [12] ZHAO S J, HUANG M, YANG F, et al. A novel wideband FSS radome with loaded inductors [C]//International Applied Computational Electromagnetics Society Symposium (ACES-China). IEEE, 2022: 1 – 2. DOI: 10.1109/ACES-China56081.2022.10065188
- [13] DANUOR P, JUNG Y B. A simple reconfigurable FSS structure for antenna beam steering applications [C]//Proceedings of International Conference on Electronics, Information, and Communication (ICEIC). IEEE, 2023: 1 – 3. DOI: 10.1109/ICEIC57457.2023.10049862
- [14] LIANG F C, WANG J B, WANG J H, et al. Influence of curvature on the transmission characteristics of cylindrical frequency selective surfaces [J]. *Journal of Changchun University of Science and Technology (natural science edition)*, 2013, 36(Z2): 65 – 66+106

Biographies

TANG Xingyang received his bachelor's degree in electromagnetic field and wireless technology from Harbin Institute of Technology, China in 2022. He is currently pursuing his master's degree in electronic information at Harbin Institute of Technology.

SUI Jia received his BE degree in electronic science and technology from the Harbin Institute of Technology, China in 2021, where he is currently pursuing his ME degree in electronic science and technology. His current research interests are the design of frequency selective surfaces and frequency selective absorber .

FU Jiahui (fjh@hit.edu.cn) received his PhD degree in information and communication engineering from Harbin Institute of Technology, China in 2005. His current research interests are the design of microwave and millimeter wave circuits, antennas, supernormal media, MEMS and EMC. He has published more than 50 relevant academic papers in domestic and foreign journals.

YANG Kaiwen received his BS degree in electronic and information engineering and PhD degree in electromagnetic fields and microwave technology from Xidian University, China in 2016 and 2021, respectively. He is currently an engineer in ZTE Corporation. His current research interests include filtering antennas and base station antennas.

ZHAO Zhipeng received his BS and PhD degrees from Xidian University, China in 2015 and 2020, and then joined ZTE Corporation. He is currently a senior RF system engineer there. His main research directions include the 5G base station, non-terrestrial networks, vehicle radar, etc.